Supporting Information for

Anomalous texture development induced by grain yielding anisotropy in Ni and Ni-Mo alloys

Lu Han[1], Lars P. H. Jeurgens[2], Claudia Cancellieri[2], Jing Wang[1], Yifei Xu[1], Yuan Huang[1], Yongchang Liu[1], Zumin Wang[1*]

[1] School of Materials Science and Engineering, Tianjin University, Tianjin 300350, China

[2] Empa, Swiss Federal Laboratories for Materials Science and Technology, Laboratory for Joining Technologies and Corrosion, Ueberlandstrasse 129, 8600 Duebendorf, Switzerland

A. X-ray photoelectron spectroscopy

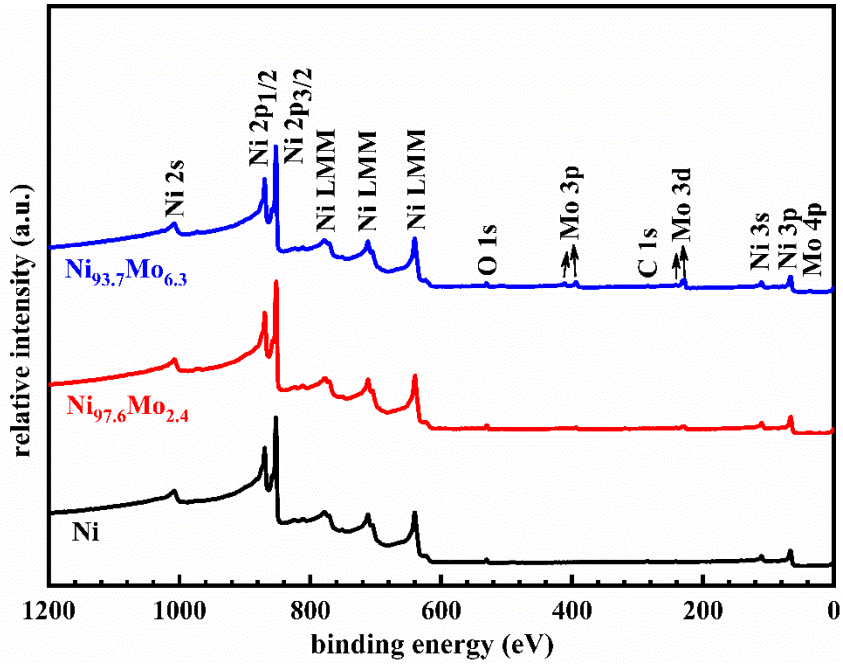

Fig. S1 XPS spectra of as-deposited Ni, $Ni_{97.6}Mo_{2.4}$ and $Ni_{93.7}Mo_{6.3}$ films.

The compositions of Ni and Ni-Mo alloy films have been investigated by X-ray photoelectron spectroscopy (XPS) in an Axis Supra system (base pressure < 2×10^{-8} Pa) using monochromatic Al Kα radiation ($h\nu$ = 1486.68 eV, analysis area 700 × 300 μm). Before each measurement, the specimen was first sputter-cleaned for 500 s by 4 keV Ar^+ to remove the

surficial native oxide layer. As evidenced by the XPS spectra in Fig. S1, the films have a high purity. Besides the dominant peaks corresponding to Ni and Mo, only a trace amount of O and C (both lower than 2 at. %) could be detected in the films.

B. Determination of the residual stress in the as-deposited Ni film

According to this so-called *d-sin*$^2\psi$ method, $d^{\{111\}}(\psi)$ is a linear function of *sin*$^2\psi$ [S1, S2],

$$\frac{d^{\{111\}}(\psi)-d_0^{\{111\}}}{d_0^{\{111\}}}=(2S_1^{\{111\}}+\frac{1}{2}S_2^{\{111\}}\times\sin^2\psi)\sigma_{//}, \tag{S1}$$

where ψ is specimen tilting angles, i.e., ψ: −10, 0, 10, and 20 °, $d_0^{\{111\}}$ is the strain-free lattice spacing of {111} planes, which is 2.034 Å (PDF card No. 04-0850); $\sigma_{//}$ is the stress parallel to the surface (in-plane); the diffraction (X-ray) elastic constants (XEC) of $S_1^{\{111\}}$ and $S_2^{\{111\}}$ can be obtained from a grain-interaction model-the Voigt model (Voigt 1910) [S2-S4], which assumes that the strain in the specimen is homogenous. In that case, the strain is the same for all crystallites, while the stress is different in differently oriented crystallite [S2].

The XECs can be calculated by single-crystal elastic compliances:

$$S_1=\frac{2S_0(S_{11}+2S_{12})+5S_{12}S_{44}}{6S_0+5S_{44}} \tag{S2}$$

$$\frac{1}{2}S_2=\frac{5(S_{11}-S_{12})S_{44}}{6S_0+5S_{44}} \tag{S3}$$

with

$$S_0=S_{11}-S_{12}-\frac{S_{44}}{2} \tag{S4}$$

S_{11}, S_{12} and S_{44} are the coefficient of single-crystal elastic compliances, which are given in Table S1.

Table S1. The coefficient of single-crystal elastic compliances [S5] and the calculated XECs.

single-crystal elastic compliances (TPa^{-1})			XEC$_s$ (TPa^{-1})	
S_{11}	S_{12}	S_{44}	S_1	S_2
7.67	−2.93	8.23	-1.21	10.90

The residual stress σ_0 of as-deposited Ni film can be calculated according to the slope of the line $d^{\{111\}}(\psi) - \sin^2\psi$. Plots of lattice spacing d as function of $\sin^2\psi$ in the as-deposited Ni film are shown in Fig. S2. The residual stress σ_0 in the Ni film was thus determined to be -0.70 GPa.

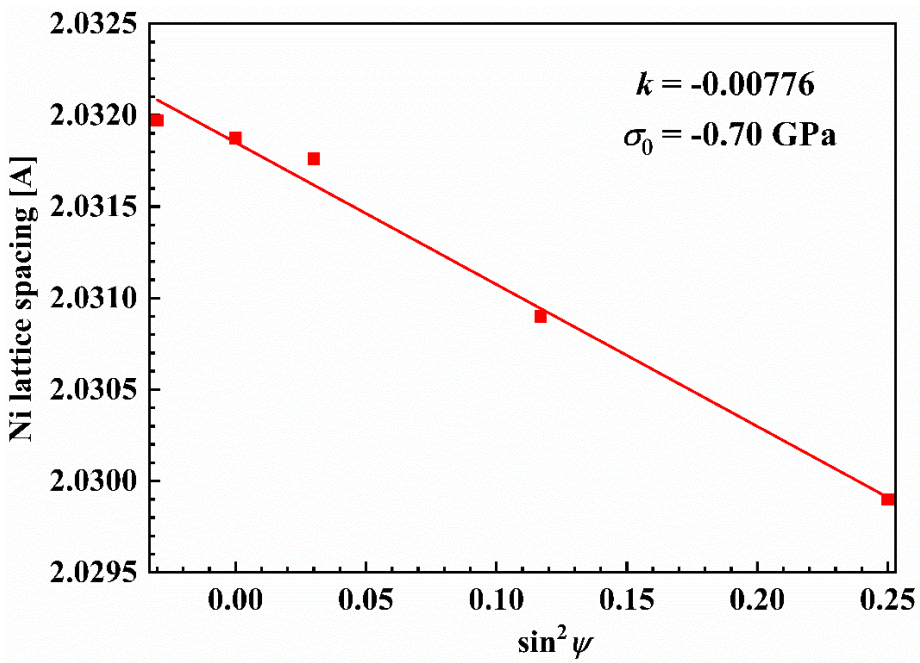

Fig. S2 Plot of $d^{\{111\}}$ lattice spacing as function of $\sin^2\psi$ for an as-deposited Ni film with the thickness of 350 nm.

C. Calculation of the biaxial elastic modulus M_{hkl} at different temperatures

The biaxial elastic modulus M_{hkl} in (111) and (100) cube planes of Ni films are isotropic and they are given by [S6]

$$M_{111} = \frac{6C_{44}\left(C_{11}+2C_{12}\right)}{C_{11}+2C_{12}+4C_{44}} \tag{S5}$$

$$M_{100} = C_{11}+C_{12}-\frac{2C_{12}^2}{C_{11}} \tag{S6}$$

The elastic properties are anisotropic in (110) plane of nickel film. The biaxial elastic modulus in mutually perpendicular [100] and [110] directions are different [S6]

$$M_{[100]} = C_{11}+C_{12}-\frac{C_{12}\left(C_{11}+3C_{12}-2C_{44}\right)}{\left(C_{11}+C_{12}+2C_{44}\right)} \tag{S7}$$

$$M_{[01\bar{1}]} = \frac{\left(2C_{11}+6C_{12}+4C_{44}\right)}{4}-\frac{\left(2C_{11}+2C_{12}-4C_{44}\right)}{4}\cdot\frac{\left(C_{11}+3C_{12}-2C_{44}\right)}{\left(C_{11}+C_{12}+2C_{44}\right)} \tag{S8}$$

$$M_{110} = \frac{\left(M_{[100]}+M_{[01\bar{1}]}\right)}{2} \tag{S9}$$

According to Eqs. (S5-S9), the biaxial elastic moduli M_{hkl} at different temperatures have been calculated. The results are shown below in Table S2.

Table S2. The components of the stiffness matrix C_{11}, C_{12} and C_{44} of Ni [S7] and the biaxial elastic modulus M_{hkl} at different temperatures.

T (°C)	C_{11} (GPa)	C_{12} (GPa)	C_{44} (GPa)	M_{111} (GPa)	M_{100} (GPa)	M_{110} (GPa)
25	250.3	123.6	150	407.97	251.83	378.98
200	240.2	116.8	149.3	396.29	243.41	368.29
400	228.2	109.1	147.8	381.52	232.98	354.74
600	216.4	101.4	145.4	365.41	222.77	340.06
700	210.5	97.7	144.1	357.26	217.51	332.60
800	204.7	93.9	143.9	350.05	212.45	326.03

D. Comparison of the yield stresses of nano-grained Ni, single-crystalline Ni films and coarse-grained Ni

Table S3. Calculated yield stresses of different families of {*hkl*} grains with a fixed nano-grain size of 50 nm (*i.e.* nano-grained Ni) in Ni films with a thickness of 350 nm on a Si substrate at different temperatures. For comparison, the calculated yield stresses of different families of {*hkl*} grains with an infinite in-plane grain size (*i.e.* single-crystalline Ni) for Ni films with a thickness of 350 nm on a Si substrate, as well as the experimental yield stress values of coarse-grained Ni (grain size > 85 μm) [S8], are also provided.

Yield Stress (MPa) / *T* (°C)	Nanograined Ni[a]			Single-crystalline Ni[b]			Coarse-grained Ni[c]
	{111}	{100}	{110}	{111}	{100}	{110}	
25	1889.1	1250.4	1223.7	126.6	73.2	51.6	97.4
200	1810.7	1198.2	1172.1	124.3	71.9	50.7	87.7
400	1714.6	1134.3	1108.9	121.5	70.2	49.5	76.3
600	1600.8	1058.6	1034.2	117.8	68.1	48.0	66.8
800	1469.1	971.0	947.8	113.3	65.4	46.1	57.6

a: calculation results in Fig. 7b.

b: (assuming an infinite grain size) calculated using Eq. (9).

c: data from Ref. [S8].

E. XRD patterns of the films annealed at different temperatures for different times

In order to obtain the peak intensity ratios of the (220) and (111) diffraction peaks for the Arrhenius analysis, the Ni, $Ni_{97.6}Mo_{2.4}$ and $Ni_{93.7}Mo_{6.3}$ films were annealed at 400, 600, 700 and 800 °C for 0.5, 1 and 2 h. The XRD patterns of as-deposited and annealed specimens are shown in Fig. S3. On this basis, the kinetics of texture transformation from {111} to {110} was analyzed.

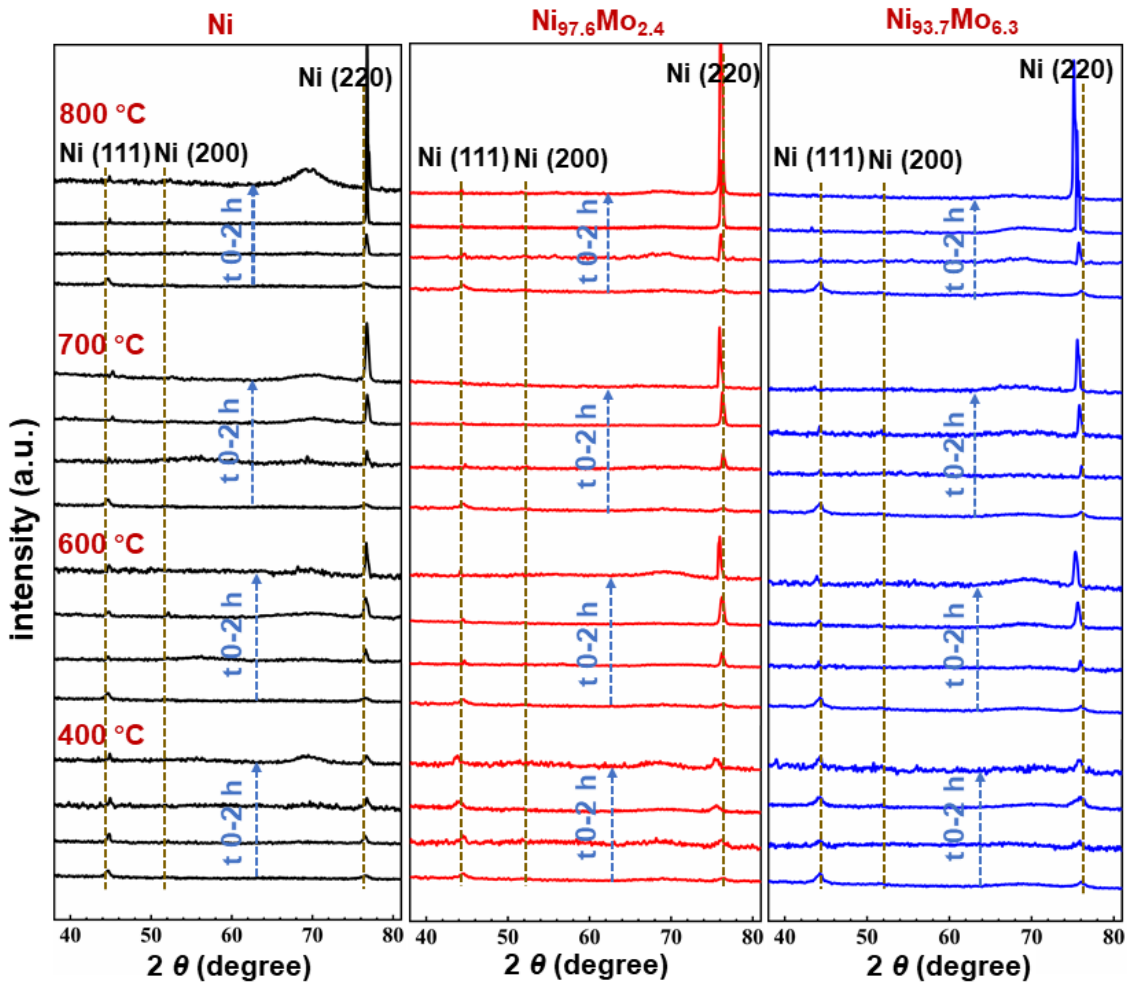

Fig. S3 XRD patterns of as-deposited Ni, $Ni_{97.6}Mo_{2.4}$ and $Ni_{93.7}Mo_{6.3}$ films, and the specimens annealed at 400, 600, 700 and 800 °C for 0.5, 1 and 2 h.

F. Model calculations of Cu and Al films on Si

The thermal expansion coefficients of Cu and Al at room temperature are 16.87 and 23.22 $\times 10^{-6}$ K^{-1}, respectively. The thermal expansion coefficients increase linearly with the increase of temperature [S9]. The thermal misfit strain $\varepsilon_{thermal}$ in Cu and Al films, as caused by the difference in the thermal expansion coefficients of the films and the substrate, was calculated using Eq. (3). The corresponding strain energy W_{hkl} (T) of Cu and Al films (with thickness of 350 nm and a fix grain size of 50 nm) at different temperatures was calculated using Eqs. (7) and (14). The biaxial elastic modulus M_{hkl} (T) of Cu [S10] and Al [S11] at different temperatures are shown in Table S4. The corresponding yield stresses of the Cu and Al films were calculated using Eq. (9), with the input parameters collected in Table S5. The surface energies of Cu and Al were calculated using Eq. (2) with the input parameters collected in Table S6.

The thus calculated elastic strain energy, as well as the sum of surface energy and strain energy, of [111], [100] and [110] oriented grains of Cu and Al films as a function of the temperature are shown in Fig. S4. It follows that, for both Cu and Al films, [110] oriented grains can also preferably grow at the expense of [100] and [111] oriented grains at high temperatures, as cause by the grain yielding anisotropy.

Table S4

The biaxial elastic modulus M_{hkl} of Cu [S10] and Al [S11] at different temperatures.

T (K)	Cu			Al		
	111	100	110	111	100	110
300	262.80	115.96	234.69	113.08	98.34	109.57
400	254.97	109.50	227.17	108.62	93.71	105.07
600	239.86	101.65	213.28	97.99	82.03	94.21
800	224.45	92.69	198.97	86.22	69.86	82.36

Table S5

Burgers vectors, Poisson's ratio [S12] and the elasticity modulus E_i of Cu [S10]and Al [S11].

metal	b (nm)	υ_i	E_i (GPa)			
			25 °C	200 °C	400 °C	600 °C
Cu	0.26	0.34	129.8	119.9	108.7	97.4
Al	0.29	0.35	73.0	61.4	52.3	48.3

Table S6

Parameters used for calculation of the surface energy of Cu and Al [S13, S14].

metal	$S^s_{<i>}$ (J/mol·K)	C_0 (10^8 mol$^{-1/3}$)	$V^s_{<i>}$ (10^{-6} m^3/mol)	$f_{<i>}$	$\gamma^s_{<i>hkl}$ (0K) (J/m^2)		
					{111}	{100}	{110}
Cu	7.72	4.5	7.14	0.35	1.952	2.237	2.166
Al			9.99	0.35	0.939	1.081	1.090

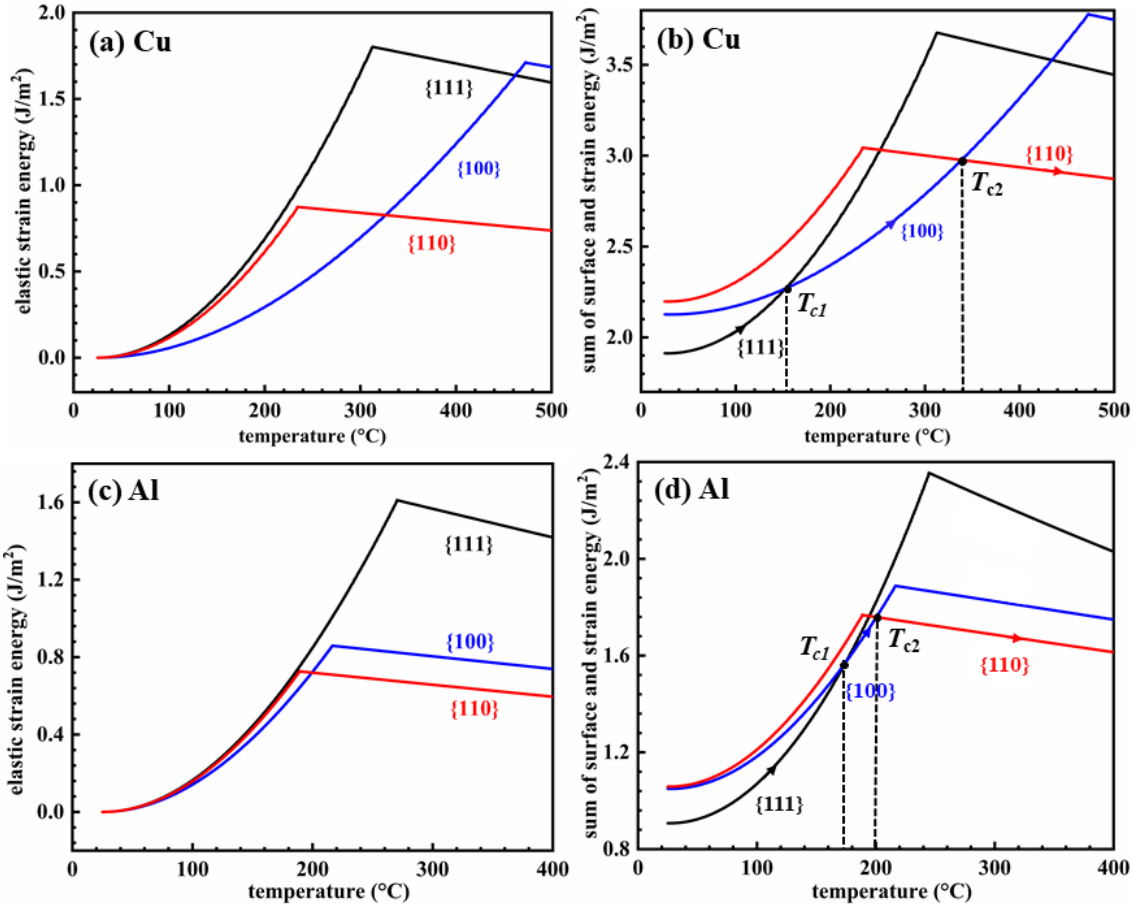

Fig. S4 Calculated elastic strain energy (a) (c), and sum of surface energy and strain energy (b) (d) of [111], [100] and [110] oriented grains of Cu and Al films as a function of the temperature.

References

[S1] Q. Luo, A.H. Jones, High-precision determination of residual stress of polycrystalline coatings using optimised XRD-sin2ψ technique, Surface and Coatings Technology 205 (5) (2010) 1403-1408.

[S2] U. Welzel, J. Ligot, P. Lamparter, A. Vermeulen, E. Mittemeijer, Stress analysis of polycrystalline thin films and surface regions by X-ray diffraction, Journal of Applied Crystallography 38 (2005) 1-29.

[S3] W. Voigt, Lehrbuch Der Kristallphysik, Leipzig: Teubner, 1910.

[S4] U. Welzel, M. Leoni, E.J. Mittemeijer, The determination of stresses in thin films; modelling elastic grain interaction, Philosophical Magazine 83 (5) (2003) 603-630.

[S5] H. Tsai, Elastic properties, damping capacity and shape memory alloys, in: T.C.T. W.F. Gale (Ed.), Smithells Metals Reference Book (Eighth Edition), Butterworth-Heinemann, Oxford, 2004, pp. 15-1-15-45.

[S6] W.D. Nix, Mechanical properties of thin films, Metallurgical Transactions A 20 (11) (1989) 2217-2245.

[S7] G.A.Alers, J.R.Neighbours, H.Sato, Temperature dependent magnetic contributions to the high field elastic constants of nickel and an Fe-Ni alloy, Journal of Physics and Chemistry of Solids 13 (1-2) (1960) 40-55.

[S8] Z. Wu, H. Bei, G.M. Pharr, E.P. George, Temperature dependence of the mechanical properties of equiatomic solid solution alloys with face-centered cubic crystal structures, Acta Materialia 81 (2014) 428-441.

[S9] R.S. Krishnan, R. Srinivasan, S. Devanarayanan, CHAPTER 5 - Thermal Expansion Data, in: R.S. Krishnan, R. Srinivasan, S. Devanarayanan (Eds.), Thermal Expansion of Crystals, Pergamon1979, pp. 115-194.

[S10] Y.A. Chang, L.J.J.o.A.P. Himmel, Temperature Dependence of the Elastic Constants of Cu, Ag, and Au above Room Temperature, 37 (9) (1966) 3567-3572.

[S11] D. Gerlich, E.S. Fisher, The high temperature elastic moduli of aluminum, Journal of Physics and Chemistry of Solids 30 (5) (1969) 1197-1205.

[S12] 15 - Elastic properties, damping capacity and shape memory alloys, in: W.F. Gale, T.C. Totemeier (Eds.), Smithells Metals Reference Book (Eighth Edition), Butterworth-Heinemann, Oxford, 2004, pp. 15-1-15-45.

[S13] L. Vitos, A. Ruban, H.L. Skriver, J. Kollár, The surface energy of metals, Surface Science 411 (1-2) (1998) 186-202.

[S14] Z. M. Wang, J. Y. Wang, L. P. H. Jeurgens, E.J. Mittemeijer, Thermodynamics and

mechanism of metal-induced crystallization in immiscible alloy systems: Experiments and calculations on Al/aGe and Al/aSi bilayers, Physical Review B 77 (4) (2008) 045424.